A comparative study of the Ruddlesden-Popper series, Lan+1NinO3n+1 (n=1, 2 and 3), for solid-oxide fuel-cell cathode applications

Amow, Gisele; Davidson, Isobel; Skinner, S. J.

Publisher's version / Version de l'éditeur:
https://doi.org/10.1016/j.ssi.2006.05.005
Solid State Ionics, 177, May, pp. 1205-1210, 2006

Available online at www.sciencedirect.com
SCIENCE DIRECT®
Solid State Ionics 177 (2006) 1205–1210
SOLID STATE IONICS
www.elsevier.com/locate/ssi

A comparative study of the Ruddlesden-Popper series, $La_{n+1}Ni_nO_{3n+1}$ ($n=1$, 2 and 3), for solid-oxide fuel-cell cathode applications

G. Amow [a,*], I.J. Davidson [b], S.J. Skinner [c]

[a] Defence Research and Development Canada-Atlantic, Ottawa, Ontario, Canada
[b] Institute for Chemical Process and Environmental Technology, National Research, Council Canada, Ottawa, Ontario, Canada
[c] Department of Materials, Imperial College London, Prince Consort Road, London, SW7, 2BP, UK

Received 9 November 2005; received in revised form 8 March 2006; accepted 3 May 2006

Abstract

A comparative investigation of the much-studied $La_2NiO_{4+\delta}$ ($n=1$) phase and the higher-order Ruddlesden-Popper phases, $La_{n+1}Ni_nO_{3n+1}$ ($n=2$ and 3), has been undertaken to determine their suitability as cathodes for intermediate-temperature solid-oxide fuel cells. As n is increased, a structural phase transition is observed from tetragonal *I4/mmm* in the hyperstoichiometric $La_2NiO_{4.15}$ ($n=1$) to orthorhombic *Fmmm* in the oxygen-deficient phases, $La_3Ni_2O_{6.95}$ ($n=2$) and $La_4Ni_3O_{9.78}$ ($n=3$). High temperature d.c. electrical conductivity measurements reveal a dramatic increase in overall values from $n=1$, 2 to 3 with metallic behavior observed for $La_4Ni_3O_{9.78}$. Impedance spectroscopy measurements on symmetrical cells with $La_{0.9}Sr_{0.10}Ga_{0.80}Mg_{0.20}O_{3-\delta}$ (LSGM-9182) as the electrolyte show a systematic improvement in the electrode performance from $La_2NiO_{4.15}$ to $La_4Ni_3O_{9.78}$ with ~1 Ω cm^2 observed at 1073 K for the latter. Long-term thermal stability tests show no impurity formation when $La_3Ni_2O_{6.95}$ and $La_4Ni_3O_{9.78}$ are heated at 1123 K for 2 weeks in air, in contrast to previously reported data for $La_2NiO_{4.15}$. The relative thermal expansion coefficients of $La_3Ni_2O_{6.95}$ and $La_4Ni_3O_{9.78}$ were found to be similar at $\sim 13.2\times10^{-6}$ K^{-1} from 348 K to 1173 K in air compared to 13.8×10^{-6} K^{-1} for $La_2NiO_{4.15}$. Taken together, these observations suggest favourable use for the $n=2$ and 3 phases as cathodes in intermediate-temperature solid-oxide fuel cells when compared to the much-studied $La_2NiO_{4+\delta}$ ($n=1$) phase.

Keywords: Ruddlesden-Popper; Solid-oxide fuel cells; Cathode; X-ray diffraction

1. Introduction

Traditionally, solid-oxide fuel cell (SOFC) cathodes are perovskite materials such as $La_{1-x}Sr_xMnO_{3-\delta}$ (LSM) or $La_{1-x}Sr_xCo_{1-y}Fe_yO_{3-\delta}$ (LSCF). However, these materials are notorious for suffering long-term mechanical and thermal degradation at the elevated operating temperatures of the fuel cell stack to the detriment of long-term performance and longevity. Consequently, current SOFC research trends point towards a lowering of stack operation temperatures to an intermediate-temperature range defined broadly as ~923 K–1073 K. From a materials point of view, this will enable increased durability of stack components both thermally and mechanically, as well as affording a greater choice of cheaper materials from which to build stack components. It is clear that first generation cathode materials based on LSM, for example, are not suitable for use in the intermediate temperature range principally due to poor oxide-ion conductivity coupled with a decrease in electronic conductivity, which are important characteristics required for the oxygen reduction process at the cathodes.

It is within this context that the Ruddlesden-Popper (RP) series of materials based on $La_2NiO_{4+\delta}$ has attracted much attention as an alternate cathode material for lower-temperature operation [1–3]. This is largely due to the improved oxide-ion conductivity observed in the $La_2NiO_{4+\delta}$ series of materials in the intermediate temperature range coupled with acceptable electrical conductivity values (~100 S/cm at 973 K) [4–6]. The Ruddlesden-Popper structure is comprised of alternating perovskite and rock-salt layers, as shown in Fig. 1. As a consequence of the layered framework, the structure can accommodate a range of hyperstoichiometry, denoted by δ, in the interstitial sites of the rock-salt layer in order to relieve the compressive stresses of the NiO_6 octahedra [7,8].

* Corresponding author. c/o National Research Council-ICPET, 1200 Montreal Road, Ottawa, Ontario, Canada K1A 0K2. Tel.: +1 613 991 2615; fax: +1 613 991 2384.
E-mail address: Gisele.Amow@drdc-rddc.gc.ca (G. Amow).

0167-2738/$ - see front matter © 2006 Elsevier B.V. All rights reserved.
doi:10.1016/j.ssi.2006.05.005

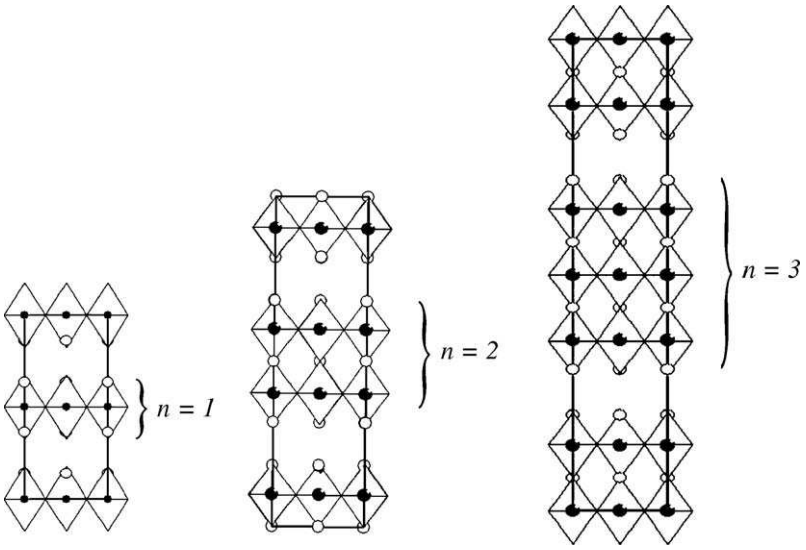

Fig. 1. Illustration of the Ruddlesden-Popper phases, $La_{n+1}Ni_nO_{2n+1}$ (n=1, 2 and 3).

Despite the enhanced oxide-ion conductivity, the electrode performance of $La_2NiO_{4+\delta}$ in symmetrical cells is poor compared to LSM and LSCF [9,10]. More detrimental, however, is the long-term thermal behavior of this material, which showed impurity Ni^{2+}/Ni^{3+} phase formation when aged at 1173 K for 2 weeks in air [11]. This degradation can be understood by recognizing that stoichiometric $La_2NiO_{4+\delta}$ (δ=0) is predominantly comprised of Ni^{2+} ions, which are stable at temperatures above 1373 K. On the other hand, the Ni^{3+} ion is favourably stable below 1173 K in air as reflected by the stability of $LaNiO_3$ below this temperature. In light of this, it is expected that the higher-ordered RP phases, $La_{n+1}Ni_nO_{3n+1}$ (n=2 and 3) would be superior candidates from a stability stance for intermediate temperature SOFCs than $La_2NiO_{4+\delta}$ given the increasing amounts of Ni^{3+} ions as one goes from n=2 to n=3. In addition, as the electronic conductivity of the Ruddlesden-Popper phases originates from the NiO_6 octahedra in the perovskite layers, it is anticipated that this physical property will also improve as increased three-dimensionality is imparted to the structure with increased n; indeed, $La_4Ni_3O_{10-\delta}$ is metallic at room temperature.

Most studies on the physical properties of the higher-order Ruddlesden-Popper n=2 and 3 phases have centred upon the anomalies observed in the electronic conductivity below room temperature, which have been associated with charge wave density instabilities [12,13]. As such, investigations of the high-temperature structural and physical properties of higher-order Ruddlesden-Popper phases are almost non-existent with only one study published on the electrical conductivity of $La_4Ni_3O_{10}$ [14]. More recently, we reported preliminary structural and physical property data of $La_3Ni_2O_{6.95}$ and $La_4Ni_3O_{9.78}$ [11] and in this paper, we present extended studies of these phases within the context of their suitability as cathodes for intermediate solid-oxide fuel cells.

2. Experimental procedure

The $La_{n+1}Ni_nO_{3n+1}$ (n=1, 2 and 3) phases were prepared by the Pechini method [15] in which stoichiometric amounts of lanthanum- and nickel-nitrate were dissolved in water to which calculated amounts of excess citric acid and ethylene glycol were added. After allowing for water evaporation on a hot plate, a gel was formed, which was dried overnight under vacuum at ~453 K. Once dried, the resulting foam-like residue was ground and pre-fired at 1023 K for 4 h in air to remove unwanted organic residues. Pellets of 25 mm diameter of each composition were made from the treated powder and single-phase materials were obtained by firing under the conditions shown in Table 1. The ramp and cooling rates used in the syntheses were 5 K/min.

A Bruker D8 X-ray diffractometer with CuKα radiation was used for phase-purity determination and structural characterization. For the latter purpose, data were collected over the range of $10° < 2\theta < 100°$, $\Delta 2\theta = 0.02°$ with t=10 s. Least-squares fitting of the data was achieved using *TOPAS* to derive unit-cell parameters [16].

To monitor structural changes as a function of temperature, data were collected on a Philips X′Pert diffractometer equipped with a Buehler HDK 2.4 high temperature stage with a platinum heating strip under static air. The samples were heated at 60°/min with an equilibration time of 5 min at each temperature of interest. Data were collected from 334 K to 1337 K in predetermined temperature steps with 2θ=10–80°, $\Delta 2\theta$=0.02° and t=1 s. The temperature of the sample chamber was calibrated using thermochromic paints.

The oxygen contents, δ, of the n=1, 2 and 3 phases were determined by thermogravimetric analysis (Setaram Setsys

Table 1
Summary of synthesis conditions and oxygen content for n=1, 2, and 3 phases

n	T (K)	Total time
1	1623	4 h
2	1373	2 days
3	1323	6 days[a]

[a] With one intermediate grinding.

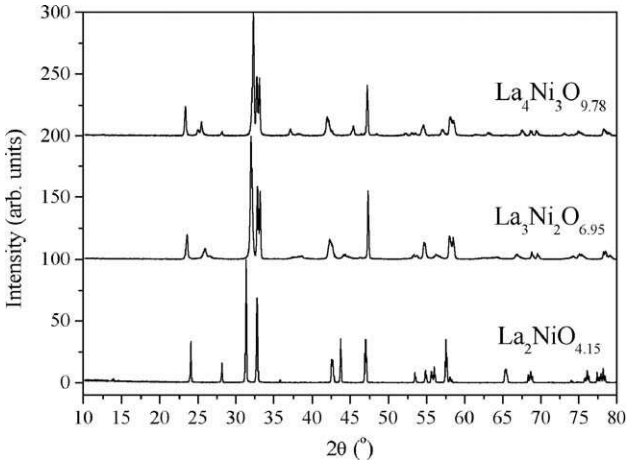

Fig. 2. X-ray diffraction patterns for $La_2NiO_{4.15}$, $La_3Ni_2O_{6.95}$ and $La_4Ni_3O_{9.78}$ at room temperature.

Evolution) under a flowing 5% H_2–argon gas mixture by heating to 1173 K at 5 K/min with a dwell time of 30 min at this final temperature. Nominal metal-ion contents were assumed throughout the calculations.

Changes in the oxygen content of the $n=1$, 2 and 3 phases were also investigated with thermogravimetric analysis (TGA) in air. For this, a TA Instruments Thermogravimetric Analyzer (TGA 2950) was used. Approximately 80–90 mg of sample were used with data collected from RT to 1173 K at 5 K/min in flowing air.

High-temperature electrical conductivity data were collected with the van der Pauw technique from an in-house built apparatus controlled by Labview software. Data were collected in a hysteretic manner from RT to 1173 K in air on square samples with typical dimensions of ~1.2 cm × 1.2 cm with a thickness of ~0.18 cm. The sample density for the $n=1$ phase was >85% theoretical density, while for the $n=2$ and 3 phases the pellets were ~58% theoretical density despite isostatic cold-pressing under 300 MPa pressure.

Thermal expansion data were collected on a TA Instruments thermomechanical analyzer (TMA 2940). The samples were made with parallel sides and on average were 10 mm long. Data were collected from RT to 1173 K at 5 K/min in air.

The electrode performances of each of these materials were evaluated in symmetrical cells with $La_{0.90}Sr_{0.10}Ga_{0.80}Mg_{0.20}O_{3-\delta}$ (LSGM-9182) as electrolyte (Praxair Specialty Ceramics). For this, two-probe a.c. impedance spectroscopy was used with an in-house built apparatus controlled by Labview. The symmetrical cells were prepared by making an ink of the powders with ethylene glycol, and brush-coating onto dense (>97% theoretical density) LSGM-9182 pellets. Typical pellet sizes were ~0.84 cm in diameter and ~1.35 mm thick. The brush-coated pellets were then fired at 1173 K for 4 h in air to promote adhesion at the electrode/electrolyte interface. Data were collected on a 1260 Solartron impedance analyzer in the frequency range of 15 MHz to 0.01 Hz from 1173 K to 723 K in static air. The amplitude of the applied potential signal was 50 mV.

Table 2
Unit-cell parameters by X-ray diffraction and oxygen content, δ

n	a (Å)	b (Å)	c (Å)	Space group	δ
1	5.4607 (2)	–	12.6862 (7)	*I4/mmm*	0.15
2	5.4040 (19)	5.4520 (19)	20.4420 (71)	*Fmmm*	−0.05
3	5.4144 (14)	5.4622 (14)	27.9748 (68)	*Fmmm*	−0.22

3. Results and discussion

3.1. Structural and oxygen content analysis

The prepared $n=1$, 2 and 3 compositions were identified as single phases by X-ray powder diffraction, as shown in Fig. 2. The unit-cell parameters and oxygen contents are summarized in Table 2. Peak indexation and unit-cell determination by least-squares fitting led to the identification of the $La_2NiO_{4+\delta}$ phase as being *I/4mmm* and orthorhombic *Fmmm* for the $n=2$ and $n=3$ phases, which is in good agreement with previous X-ray powder diffraction studies in the literature [12,13,17]. Thermogravimetric analysis under a reducing atmosphere of a 5% H_2–Ar gas mixture showed the $n=1$ phase to be oxygen hyperstoichiometric with a composition of $La_2NiO_{4.15}$, while the $n=2$ and 3 phases were found to be oxygen deficient at $La_3Ni_2O_{6.95}$ and $La_4Ni_3O_{9.78}$ and is in agreement with similar compositions previously prepared by a nitrate method [17]. Also of interest is the comparative behavior of the $n=1$, 2 and 3 phases in air on heating, which shows an initial weight gain for the $n=1$ phase until ~630 K after which continuous oxygen loss is observed. For the $n=2$ and 3 phases, immediate oxygen loss is observed on heating in air up to 1173 K, see Fig. 3.

3.2. Thermal expansion

Dilatometric data for the Ruddlesden-Popper phases in this study are shown in Fig. 4. After correcting the data to take into account the thermal expansion of the sample stage, the thermal

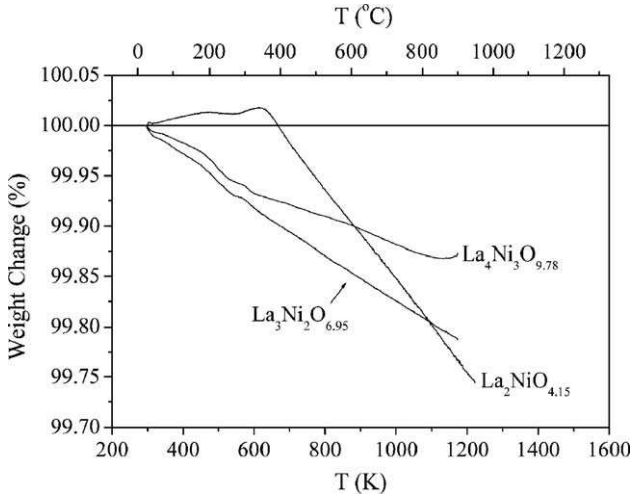

Fig. 3. Thermogravimetric analysis for $La_2NiO_{4.15}$, $La_3Ni_2O_{6.95}$ and $La_4Ni_3O_{9.78}$ in air.

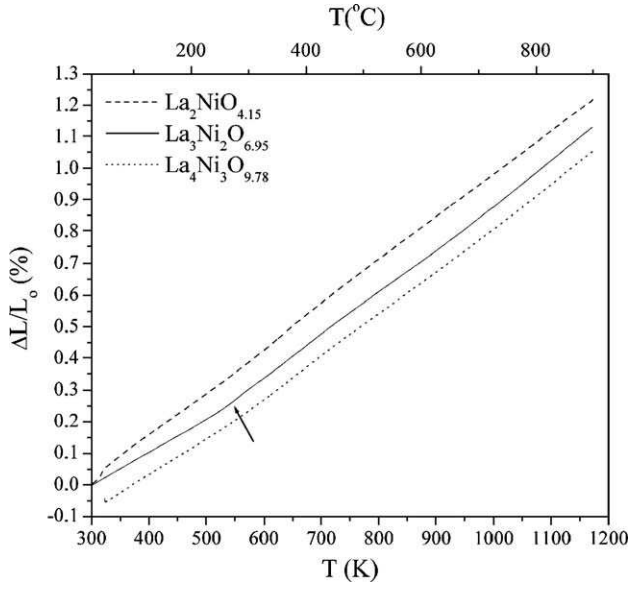

Fig. 4. Thermal expansion data for $La_2NiO_{4.15}$, $La_3Ni_2O_{6.95}$ and $La_4Ni_3O_{9.78}$ from RT to 1173 K.

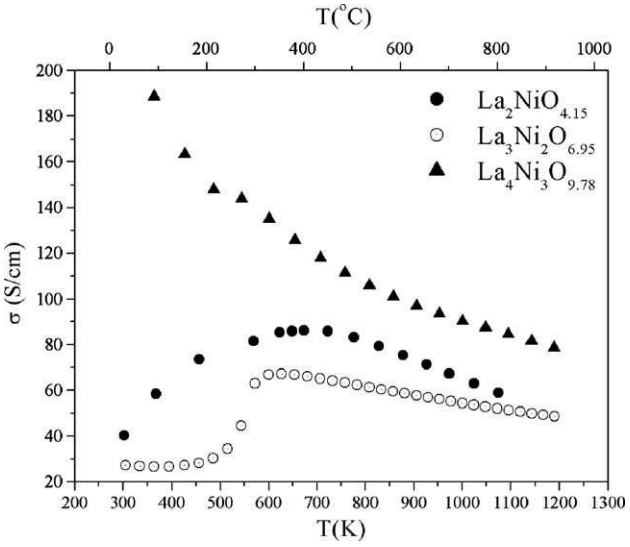

Fig. 5. Electrical conductivity vs. temperature for $La_2NiO_{4.15}$, $La_3Ni_2O_{6.95}$ and $La_4Ni_3O_{9.78}$ from RT to 1173 K in air.

expansion coefficients, α, from 348 K to 1173 K were found to be 13.8×10^{-6} K^{-1} for $La_2NiO_{4.15}$, which is in agreement with previous literature values [2,18] and $\sim13.2\times10^{-6}$ K^{-1} for both $La_3Ni_2O_{6.95}$ and $La_4Ni_3O_{9.78}$. On closer inspection, however, a subtle non-linearity in the data is observed for each composition over this temperature range. Instead, two linear regions are observed for each data set with the most distinctive change in slopes being observed for $La_3Ni_2O_{6.95}$ at ~548 K and is reflected by the different values obtained for α when the data is fitted over the temperature ranges 348 K–548 K and 548–1173 K, which are summarized in Table 3. The change in α over these two temperature regions is likely to be structural in origin and may have implications for cathode use. Furthermore, the anomaly at 548 K was found to manifest itself in other measurements such as thermogravimetric analysis, see Fig. 3, as well as the electrical conductivity behavior, which is discussed in the following section.

3.3. Electrical conductivity

The temperature dependences of the electrical conductivity for $La_2NiO_{4.15}$, $La_3Ni_2O_{6.95}$ and $La_4Ni_3O_{9.78}$ are shown in Fig. 5. It is to be noted that, given the relatively low reaction temperatures required to obtain the $n=2$ and 3 phases, the densities of the pellets used for this measurement were significantly smaller (~58%) than $La_2NiO_{4.15}$ (~85%) despite cold pressing at 300 MPa. Being mindful of this, it can be argued that the overall values for the electrical conductivity increase systematically as n increases. This trend mirrors that of the low-temperature behavior [12,13] and is not entirely unexpected. The NiO_6 octahedral units in the perovskite layers govern the electronic conduction pathways in the Ruddlesden-Popper phases [13]. Reasonably, with an increase in the number of perovskite layers, the number of conduction pathways increases leading to an enhanced observed electrical conductivity. The $La_4Ni_3O_{9.78}$ phase is metallic, whose electrical conductivity

Table 3
Thermal expansion coefficients for $La_2NiO_{4.15}$, $La_3Ni_2O_{6.95}$ and $La_4Ni_3O_{9.78}$ from 348 K to 1173 K in air

Composition	T (K)	$\alpha\times10^{-6}$ (K^{-1})
$La_2NiO_{4.15}$	348–1173	13.8
	348–548	13.1
	548–1173	13.8
$La_3Ni_2O_{6.95}$	348–1173	13.2
	348–548	10.5
	548–1173	13.7
$La_4Ni_3O_{9.78}$	348–1173	13.1
	348–548	11.2
	548–1173	13.5

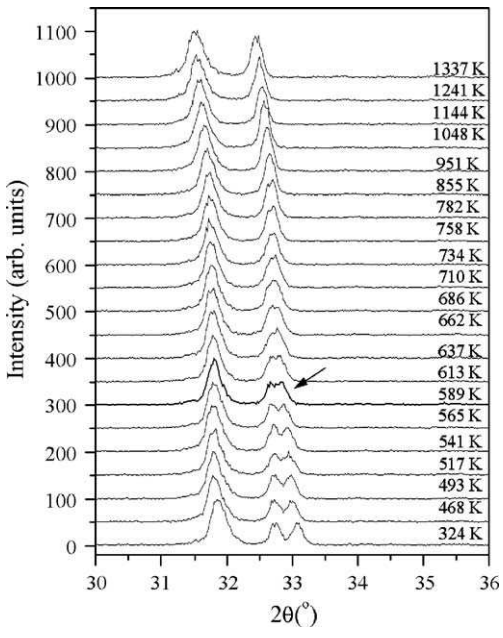

Fig. 6. High-temperature X-ray diffraction pattern for $La_3Ni_2O_{6.95}$ illustrating possible change in symmetry from orthorhombic to tetragonal at 589 K.

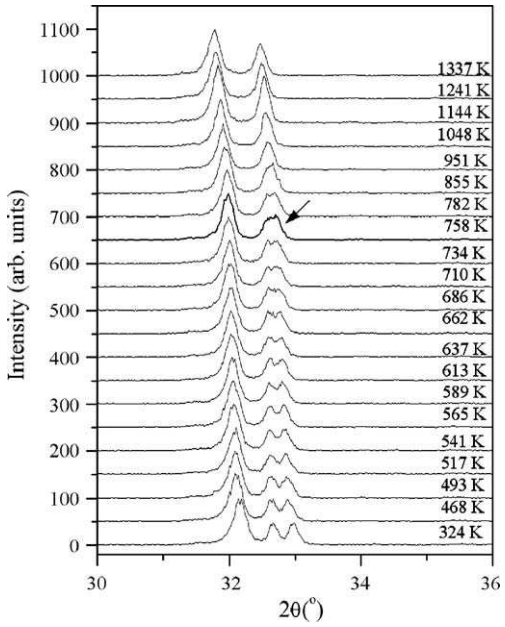

Fig. 7. High-temperature X-ray diffraction pattern for $La_4Ni_3O_{9.78}$ illustrating possible change in symmetry from orthorhombic to tetragonal at 758 K.

decreases monotonically as the temperature increases. Also, anomalies are observed at ~548 K for $La_3Ni_2O_{6.95}$ and $La_4Ni_3O_{9.78}$, which appear to coincide with the change in slope observed in the thermal expansion and the anomalies in the thermogravimetric data in air as mentioned in the previous section.

To establish whether the anomalies observed in the electrical conductivity of $La_3Ni_2O_{6.95}$ and $La_4Ni_3O_{9.78}$ are indeed structural in origin, preliminary high-temperature X-ray diffraction studies were carried out from RT to 1173 K at various temperature intervals in air, as shown in Figs. 6 and 7. Recall that both of these phases are orthorhombic *Fmmm* at RT. For both phases, transformation to a higher symmetry tetragonal phase is observed. In the case of $La_3Ni_2O_{6.95}$, the phase transition is marked by the evolution of the doublet (020, 200) peak to a singlet peak at ~589 K (see Fig. 6), which corresponds reasonably to where the anomalies are observed in the electrical conductivity, thermal expansion and thermogravimetric data.

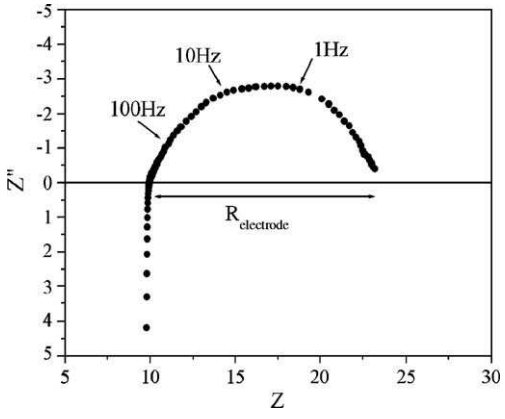

Fig. 8. Typical Nyquist plot for a higher-order Ruddlesden-Popper phase ($La_4Ni_3O_{9.78}$).

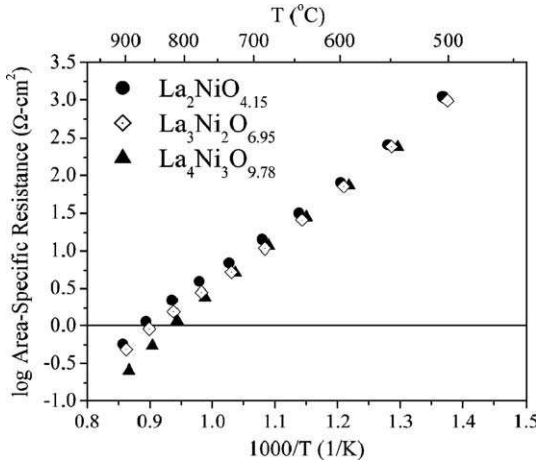

Fig. 9. Log (area-specific resistance) vs. 1000/*T* for $La_2NiO_{4.15}$, $La_3Ni_2O_{6.95}$ and $La_4Ni_3O_{9.78}$.

Curiously and less clear, however, is the apparent non-correlation for the $La_4Ni_3O_{9.78}$ phase where the singlet appears to occur much later at ~758 K. Given the inherent challenges associated with obtaining accurate geometrical bond information for such oxides with X-ray powder diffraction, attempts to accurately correlate the data with electronic transport mechanisms are difficult and was not attempted here.

3.4. Electrode performance

To determine the suitability of these materials for SOFC cathode use, impedance measurements were carried out on symmetrical cells made with LSGM-9182 as the electrolyte. A typical Nyquist plot at 1073 K is shown in Fig. 8 and the normalized area-specific resistance (ASR) values for each symmetrical cell are shown in Fig. 9. From the data, the $La_4Ni_3O_{9.78}$ coated pellet yielded the lowest area-specific resistance of ~1 Ω cm^2 at 1073 K with an activation energy of E_a=1.36 eV followed by $La_3Ni_2O_{6.95}$ and $La_2NiO_{4.15}$ with E_a=1.27 eV and 1.24 eV respectively. These values for the ASR are acknowledged to be high and will of course be dependent on the processing of the cathode layers. In this study

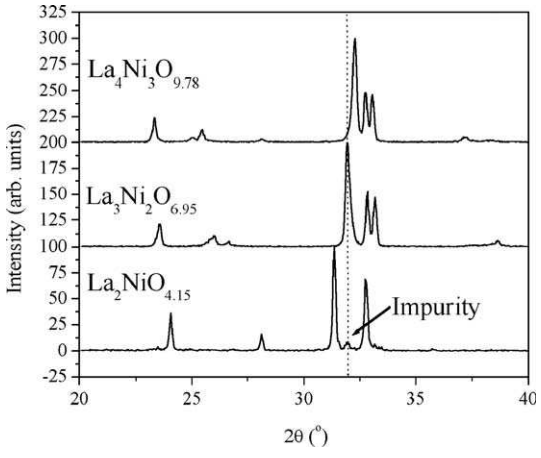

Fig. 10. Impurity phase formation for $La_2NiO_{4.15}$ after heating at 1173 K for 2 weeks in air.

each of the cathodes was processed in a consistent manner and therefore this data set is comparable. It is likely that further optimization of the cathode layers in terms of their microstructure, porosity and thickness would improve the performance of each cathode. Despite this, the observed trend correlates with the in-